Journal Pre-proof

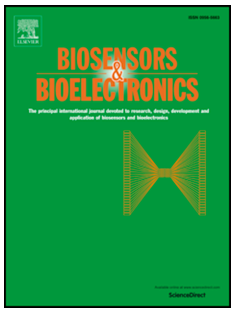

Polydopamine-gold composite-based electrochemical biosensor using dual-amplification strategy for detecting pancreatic cancer-associated microRNA

SSu-Chia Chen, Kuan-Ting Chen, Amily Fang-Ju Jou

PII: S0956-5663(20)30801-0

DOI: https://doi.org/10.1016/j.bios.2020.112815

Reference: BIOS 112815

To appear in: *Biosensors and Bioelectronics*

Received Date: 14 September 2020

Revised Date: 8 November 2020

Accepted Date: 9 November 2020

Please cite this article as: Chen, S.-C., Chen, K.-T., Fang-Ju Jou, A., Polydopamine-gold composite-based electrochemical biosensor using dual-amplification strategy for detecting pancreatic cancer-associated microRNA, *Biosensors and Bioelectronics* (2020), doi: https://doi.org/10.1016/j.bios.2020.112815.

CRediT author statement

Dr. Amily Fang-Ju Jou: Conceptualization, Methodology, Supervision, Visualization, Writing- Original draft preparation, Reviewing and Editing. **Mr. SSu-Chia Chen**: Investigation, Formal analysis, Software. **Ms. Kuan-Ting Chen**: Investigation, Formal analysis, Software.

Polydopamine-gold Composite-based Electrochemical Biosensor Using Dual-amplification Strategy for Detecting Pancreatic Cancer-associated MicroRNA

SSu-Chia Chen[†], Kuan-Ting Chen[†], and Amily Fang-Ju Jou[*]

Department of Chemistry, Chung Yuan Christian University, No. 200, Chung Pei Road, Chung Li District, Taoyuan City 320314, Taiwan (ROC)

Manuscript submitted to *Biosensors and Bioelectronics*

*Correspondence should be addressed to Amily Fang-Ju Jou (afjjou@cycu.edu.tw); [†]Authors made equal contributions to the study.

Abstract

Herein, we developed a dual-amplification-boosted, translational electrochemical biosensor for the detection of pancreatic cancer-associated microRNA, miR-196b. A biosensing event occurred when a hairpin target probe recognized miR-196b as a result of the opening of an electrode hairpin probe on a polydopmine-gold (PDA-Au) composite-modified screen-printed carbon electrode. The PDA-Au composite was synthesized in a alkaline condition where dopamine polymerized into polydopamine while gold(III) ion was *in-situ* reduced to gold nanoparticle, characterized by FT-IR, SEM, cyclic voltammetry and gel electrophoresis. The electrode modifier, PDA-Au, provided a functionalizable interface for the sensitization of electrode probes; besides, a suitable hydrophilic interface for an aqueous biosensing reaction, confirmed by water contact angle measurement and cyclic voltammetry. Confirmed by UV-VIS analyses and gel electrophoresis, the single polymerase created a dual amplification by target-recycling and generation of an catalytic DNAzyme product on the electrode probe-functionalized PDA-Au@SPCE. The isothermal, dual amplification was thereby translated into a TMB/H_2O_2-resulted electrochemical signal, acquired by scan wave voltammetry for quantifying target miR-196b. The novel electrochemical biosensor offered a detection limit of 0.26 pM, with a nice analytical reproducibility by CV (coefficient of variance) value of 8.5 ± 3.1%, and a recovery rate of 105 ± 4.1% obtained from a spiked, real human serum sample. The proposed biosensor showed great promise as a complementary tool for real sample detection in the clinic.

Keywords: microRNA, electrochemistry, biosensor, DNA, amplification

1. Introduction

Pancreatic cancer is one of the few aggressive cancers because not many symptoms appear until it reaches advanced stages (Evans et al. 2014; Rawla et al. 2019). Due to the location of pancreas sitting behind the stomach, the symptoms are very often misdiagnosed with stomach diseases, suggesting the lack of typical early symptoms to signal pancreatic cancer. However, an early detection together with proper medical treatments has been recognized to greatly improve the survival rate of patients with cancers (Chandra et al. 2017). In light of this, it is of importance to develop a sensitive screening tool based on an easily-assayed biomarker for the "silent-killer" pancreatic cancer. In response, circulating microRNAs (miRNAs), 18 – 24 nucleotide-long nucleic acids, appear to be a reliable biomarker based on their biological malfunctions implicating in cancers (Bryant et al. 2012; Heneghan et al. 2010; Kawaguchi et al. 2013; Mitchell et al. 2008). MicroRNA-196b (miR-196b) overexpression has shown clinical relevance as an independent pancreatic cancer signature, which may serve as an optimistic biomarker in a selective assay for pancreatic cancer (Gilles et al. 2018; Kanno et al. 2017; Wang et al. 2017).

DNA nanotechnology has greatly revolutionized the employability of biological chemistry in diagnostics and therapy due to sequence designability and structural dynamics. The merits enables a programmable and signal amplification detection regime for a specific, low-concentration of target, such as catalytic hairpin amplification (CHA) (Dai et al. 2017; Zheng et al. 2012), hybridization chain reaction (HCR) (Choi et al. 2014; Ge et al. 2014), exponential amplification (EXPAR) (Ye et al. 2019; Zhang 2019), rolling circle amplification (RCA), (Ali et al. 2014; Wen et al. 2012; Xing et al. 2013) and even the newly-developed CRISPR (Clustered Regularly Interspaced Short Palindromic Repeat) editing technology (Liu et al. 2020; Wang et al. 2020). In addition, colorimetric, fluorometric, acoustic and electrochemical readout fashions are easily incorporated to the detection regimes (Qualliotine et al. 2019). In particular, several merits of electrochemical

biosensors include low-cost, disposability, portability, miniaturization and user-friendly for operation, which show superior versatility over the other fashions of biosensors in the mainstream development of point-of-care testing (Christodouleas et al. 2018; Lan et al. 2016; Pallela et al. 2016; Soper et al. 2006; Zhu et al. 2013). Therefore, in this study, an isothermal, dual signal amplification strategy is designed to translate a biosensing event for miR-196b into electrochemical signals. The translational platform is based on the synthesis of a novel modifier of polydopamine-gold nanoparticle composite for fabricating a disposable screen-printed electrode (PDA-Au@SPCE). The polymeric form of PDA, obtained from a self-polymerization in alkaline solution, has attracted many research focuses because of excellent adhesion to many substrates (Lee et al. 2007; Ryu et al. 2018). As a result, a PDA-Au composite, prepared by *in-situ* reduction of gold nanoparticle, is expected to combine the advantages of the adhesion behaviors and fouling resistance of PDA films, as well as the enhanced conductivity of gold nanoparticles (Janovák and Dékány 2010). Besides, the PDA-Au composite modifier renders the working electrode of a SPCE a hydrophilic and functionalizable surface for a hairpin-structured electrode probe grafting so as to translate a biosensing event. The biosensing event between the target miR-196b and the target probe, is able to trigger the electrode probe to polymerize into a guanine-rich sequence for TMB/H_2O_2 enzyme-like catalysis reaction that can be subsequently measured by electrochemical analysis. In addition, the polymerization of the electrode probe concurrently displaces the pre-hybridized target miR-196b, creating a target-recycling amplification for improved detection sensitivity. The newly translational electrochemical biosensor aims to provide an alternative point-of-care testing tool for better understanding of the relationship of relevant miRNAs with pancreatic cancer.

2. Experimental

2.1 Chemicals and materials

All chemicals were of reagent grade. Dopamine hydrochloride, urea, sulfuric acid (H_2SO_4), hexaaminеruthenium(III) chloride ($[Ru(NH_3)_6]Cl_3$), potassium hexacyanoferrate(III) ($K_3Fe(CN)_6$), hydrogen peroxide (H_2O_2), gold(III) chloride trihydrate ($HAuCl_4 \bullet 3H_2O$), human serum from male AB plasma were obtained from Sigma–Aldrich (St. Louis, MO, USA). SYBR Gold and GeneRuler Ultra Low Range DNA ladder were purchased from Thermo Scientific (Rockford, IL, USA). Potassium phosphate dibasic (K_2HPO_4), potassium phosphate monobasic (KH_2PO_4), magnesium chloride ($MgCl_2$), tris(hydroxymethyl)aminomethane (Tris base), sodium chloride (NaCl), and potassium chloride (KCl), were obtained from J.T. Baker (Phillipsburg, NJ, USA). Klenow fragment (3’ -> 5’ exo) and 10× CutSmart buffer were obtained from New England Biolab Inc. (Ipswich, MA, UK). dNTP was purchased from Roche (Indianapolis, Indiana, USA). Polyacrylamide (29:1), ammonium persulfate (APS), tetramethylethylenediamine (TEMED) were acquired by Cyrusbioscience Inc. (Taipei, Taiwan). Enhanced K-Blue Substrate (TMB; H_2O_2 included) was purchased from Neogen Corp (Lexington, KY, USA). Disposable screen-printed carbon electrodes (SPCE, 50 $\times$ 13 mm; 3 mm-diameter of working electrode disk), included a carbon working electrode, a carbon counter electrode, and a silver pesudoreference electrode, were acquired from Zensor R&D (Taichung, Taiwan). All solutions were prepared using distilled deionized (D.D.) water having resistivity of not less than 18MΩ cm^{-1} (Purity, Prema, Taiwan). All oligonucleotides were purchased from Integrated DNA Technologies (Coralville, IA, USA) and used as provided. A stock concentration of 0.1 mM for all the oligonucleotides was prepared in a PB buffer (10 mM K_2HPO_4/KH_2PO_4, pH = 7). Hairpin-structured probes stock solutions (1×10^{-5} M, either target probes, or electrode probes) were prepared at 10 mM PBS (pH = 7, containing 150 mM NaCl and 5 mM $MgCl_2$), and formed under a slow-annealing process in which

the temperature was initially elevated to 95 ^{o}C, and followed by gradual cooling to ambient temperature using a thermocycler (T-100, BIO-RAD, USA).

2.2 Characterizations

Contact angle measurement was carried out to visualize the behavior of a water droplet that was accordingly casted on a bare SPCE, PDA@SPCE, PDA-Au@SPCE, and AuNPs@SPCE. The AuNPs@SPCE was prepared by eletrodeposition of chloroauric acid using chronoamperometry. 40 µL of gold(III) chloride trihydrate (1 mM, prepared in 0.1 M KCl aqueous solution) was used to cover the three-electrode under a constant potential of −0.66 V for 60 s, and was dried under a stream of gaseous nitrogen after rinsing with D.D. water(Jou et al. 2017). Cyclic voltammetry (CV), scan wave voltammetry (SWV), and chronoamperometry (i-t) were conducted using a CHI 1007C electrochemical analyzer/workstation (CH Instruments, Austin, TX). Cyclic voltammetry was used to study the behavior of the electroactive redox probes in a on the different modified. 5 mM of electroactive redox probes, a ferrocyanide/ferrocyanide pair $Fe(CN)_6^{3-/4-}$ or hexaammineruthenium(III) chloride, were prepared in a 10 mM PBS, pH = 7 containing 0.1 M KCl. 40 µL of the redox probe solutions was employed to cover the three-electrode, scanning from 0.8 V to −0.8 V (0.2 V to −0.8 V for $Ru(NH_3)_6^{2+/3+}$ at a scan rate of 0.1 V/s. Electrophoresis gel images were analyzed by Gel Doc^{TM} EZ Gel Imager BIO-RAD (Hercules, CA, USA). The gels were run with a 15% acrylamide solution (prepared from 29:1 acrylamide:bisacrylmaide) in a 0.5 × TBE buffer at a constant voltage of 80 V for 120 min. The gel was then stained with SYBR Gold dye to signal the band position, illuminated under UV light, and images were taken with a build-in digital camera.

2.3 Synthesis of PDA-Au composites

PDA-Au composites were synthesized by reacting dopamine (4 mmol) and gold(III) chloride trihydrate (0.1 mmol) in a alkaline Tris buffer (pH 8.5, 10 mM) at 37 ^{o}C for 1 hr. Polydopamine polymer film was also synthesized using the same condition as a control group. The as-synthesized PDA-Au composite was characterized using field emission scanning electron microscope (FESEM, JEOL, JSM-7600F, Japan) and Fourier transformation infrared spectroscopy (FT/IR-460Plus, JASCO, Japan).

2.4 Construction of PDA-Au@SPCE

6 µL of the as-synthesized PDA-Au composite was used to fully cover the working electrode of a screen-printed carbon electrode (SPCE) and left air-dried at 37 ^{o}C for 1 hr. The resulting PDA-Au@SPCE was washed using D.D. water and dried under a stream of gaseous nitrogen.

2.5 Sensitization of PDA-Au@SPCE by electrode probe

A PDA-Au@SPCE was sensitized by amine-functionalized electrode probes (EP) via glutaraldehyde-assisted linkage. The working electrode of PDA-Au@SPCE was first treated with 3 µL of glutaraldehyde (4%, prepared in a 10 mM PB, pH = 7) at 37 ^{o}C for 1 hr, and was reacted with hairpin-structured amine-EP (3 µL, 2×10^{-6} M, in 10 mM PBS, pH = 7, containing 150 mM) after the removal of excess glutaraldehyde, for another 1 hr at 37 ^{o}C to complete the preparation of EP/PDA-Au@SPCE. The resulting EP/PDA-Au@SPCE, after rinsed with 10 mM PB buffer (pH = 7) and dried under a stream of gaseous nitrogen, was ready to use.

2.6 UV-VIS absorption measurements

A synthetic TP/e-EP duplex solution (both strands were 1×10^{-6} M) was prepared in a CutSmart buffer (pH 7.9, 200 mM Tris-acetate, 500 mM potassium acetate, 100 mM magnesium acetate, 1

mg/mL bovine serum albumin) in advance. A de-hybridization reaction was performed by subjecting the as-prepared TP/e-TP duplex solution (25 μL, 1×10^{-6} M) to an equal volume of urea with a final concentration of 1 M. After gentle mixing, hemin (1×10^{-6} M, containing 0.1 M KCl) was introduced to the mixture and reacted at 37 ^{o}C for 30 min. The catalytic reaction was subsequently conducted by an addition of 10 μL TMB/H_2O_2 solution, and reacted at 37 ^{o}C for 60 min. A successful catalytic reaction was then observed as the solution turned blue, and the reaction was terminated by an addition of an aliquot of H_2SO_4 solution (10 μL, 1M), thereby resulting in a yellow-colored solution. The absorption spectrum was recorded by a Cary 60 UV-VIS spectrophotometer (Agilent Technologies). A spectrum was recorded from 600 nm to 310 nm of wavelength, and the characteristic peak at 450 nm was used for the quantification of the yellow product.

2.7 Dual-amplification strategy on the biosensing of target miR-196b

Biosensing of the specified concentration of target miR-196b was carried out on a as-prepared EP/PDA-Au@SPCE by reacting in a mixture solution (5 μL) that contained target probes (TP, 500 nM), Klenow fragment (KF, 0.05 U/μL), dNTP (0.1 mM) in a CutSmart buffer (pH 7.9, 200 mM Tris-acetate, 500 mM potassium acetate, 100 mM magnesium acetate, 1 mg/mL Bovine serum albumin) at 37 ^{o}C for 120 min. After the translational biosensing event on the electrode, an addition of urea solution (1 M) was employed to release the KF-assisted elongated electrode probe from the bulky target miR-196b/TP/EP duplex at 37 ^{o}C for 30 min, followed by a standard wash-and-dry procedure, that is, rinsing with 10 mM PB buffer (pH = 7), and dried with a stream of gaseous nitrogen. 6 μL of hemin (1×10^{-6} M, in a 10 mM PBS, pH = 7, containing 150 mM KCl) was used to assist in the self-assembled hemin/G-quadruplex DNAzyme configuration by a 30 min-incubation at 37 ^{o}C, followed by a standard wash-and-dry procedure. An aliquot of TMB/H_2O_2 mixture (40 μL, containing 0.1 M KCl) was placed onto the resulting electrode, and the electrochemical signal was recorded by

scanning wave voltammetry (SWV), scanning from 0.6 V to –0.1 V, under a 25 mV pulse at a frequency of 15 Hz.

2.8 Extraction of target miR-196b from spiked human biological serum samples

The miR-196b spiked serum samples were prepared by adding 0.7 attomol synthetic miR-196b into 200 µL of undiluted human serum sample obtained from male AB plasma (Sigma, USA), and the spiked-miR 196b was extracted according to the manufacturer's protocol using a miRNAeasy serum/plasma kit (Qiagen; Valencia, CA), which was described in the previous study (Jou et al. 2017). Briefly, an aliquote of Qizaol lysis reagent was used to dissociate the nucleoprotein complex in the spiked serum sample, followed by a serial extraction using chloroform and ethanol. After elution using double-distilled water via a spin-column as provided by the manufacturer, the obtained extract (14 µL) was stored in –20 ^{o}C prior to the detection using the current biosensor. A recovery rate was used to study the performance of the biosensor in analyzing human biological samples, in comparison with buffer solution.

3. Results and Discussion

3.1 Characterization of PDA-AuNPs composites

Scheme 1A illustrates the construction of PDA-AuNPs composite. The polydopamine (PDA) film was formed in a alkaline condition, where *in-situ* reduction of Au(III) particles via amino and catechol groups of the resulting PDA film.(Luo et al. 2014; Xu et al. 2017; Zhang et al. 2017) SEM images showed the bulk PDA film had consistent star-shaped blanks (**Figure 1A**), forming a porous membrane nanostructure.(Wei et al. 2017) In **Figure 1B**, the embedded gold nanoparticles in the PDA-AuNPs composite were uniform in size, with an average diameter of 23.5 ± 0.8 nm (calculation from 100 particles). Fourier transform infrared spectroscopy (FT-IR) was also used to investigate both the PDA film and PDA-AuNPs composite. Positions of the featured bands of the PDA film were consistent with those recorded in the literature,(Luo et al. 2015; Zangmeister et al. 2013) as indicated in **Figure 1C**. The FT-IR spectrum of PDA-AuNPs composite exhibited the similar featured bands as for the PDA film. Features that were assigned to stretching ν(O-H) and ν(N-H) at 3350 – 3450 cm^{-1} indicated catechol and amino groups, respectively, for the PDA film; however, a less broader band was observed for PDA-Au composite, suggesting a slight decrease in the amount of catechol groups. On the other hand, a new peak appearing at 1630 cm^{-1} of C=O group depicted the presence of quinone group as a result of the oxidation of catechol group, while Au (III) was reduced to Au. Such the characteristics implied a successful formation of PDA-AuNPs composite, and the *in-situ* reduction of Au (III) did not extensively affect the structure of the PDA film. Also, taking advantages of the adhesion behavior and fouling resistance due to the featured hydrophilic catechol and amino groups of PDA-Au composite, the PDA-Au composite may serve as an excellent modifier permitting the construction of disposable screen-printed carbon electrode-based (SPCE) biosensing platform, where an image of SPCE was shown in Figure S1.

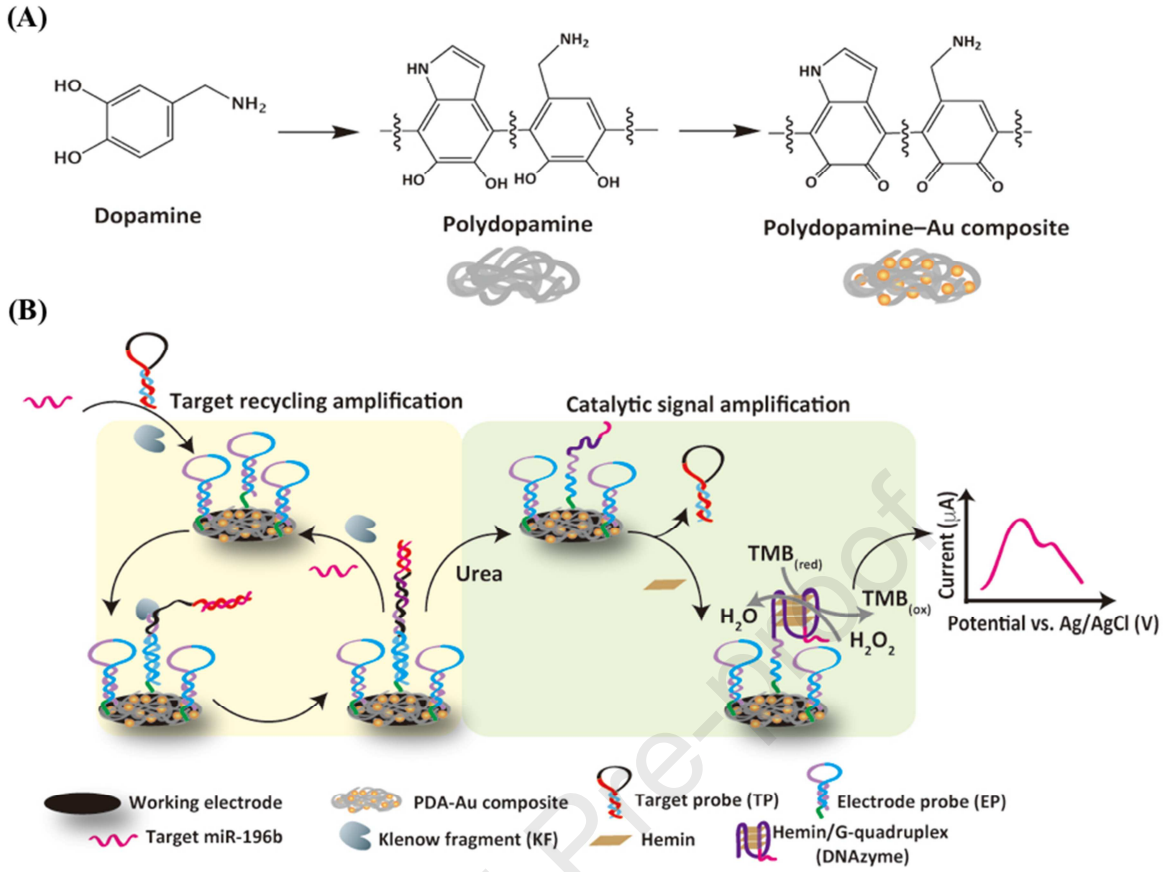

Scheme 1. Schematic illustration of **(A)** the synthesis of PDA-Au composite and **(B)** the PDA-Au modified screen-printed carbon electrode that was employed for translational biosensing of target miR-196b via dual-signal amplification.

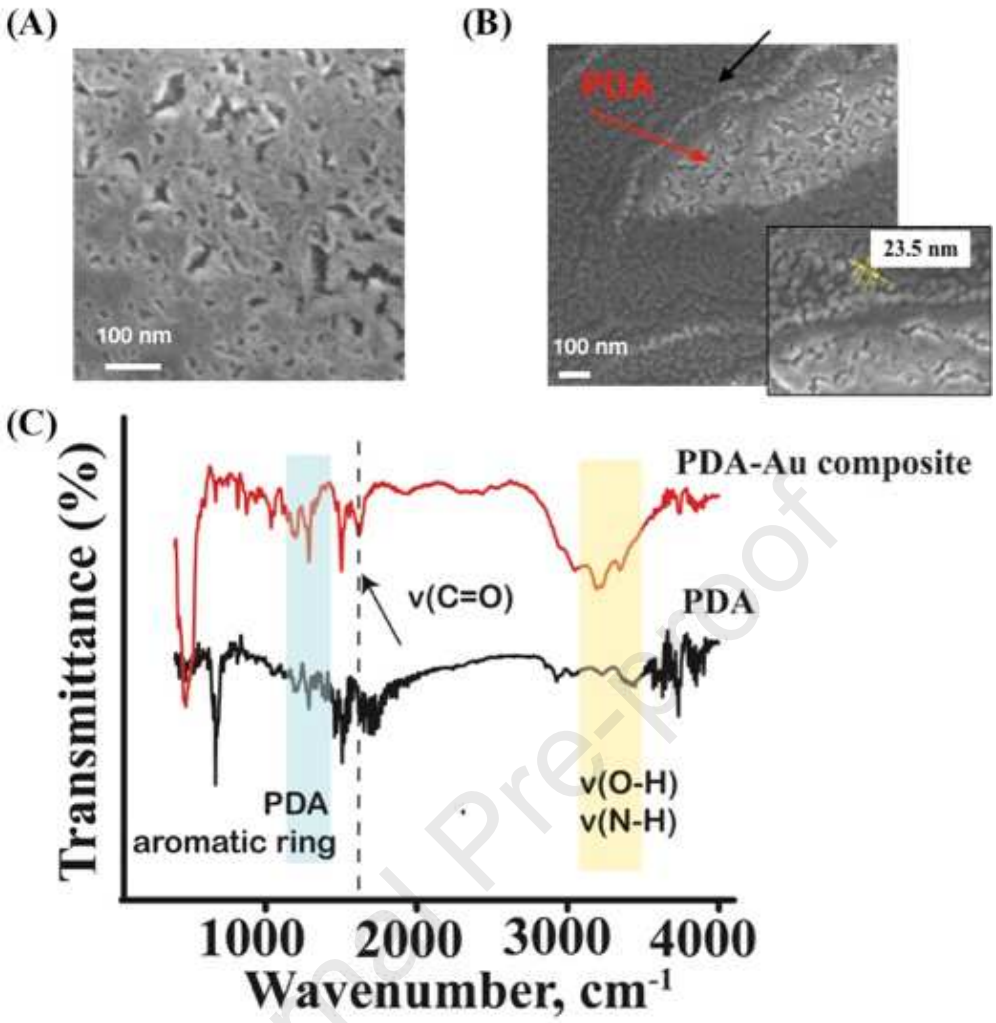

Figure 1 SEM images of **(A)** PDA film and **(B)** PDA-Au composite with a magnified image of gold nanoparticles (black arrow). **(C)** FT-IR spectra of PDA and PDA-Au composite.

3.2 Construction of PDA-AuNPs composite-modified SPCE (PDA-Au@SPCE)

Since a biosensing event occurs in aqueous phase, it is important for the working electrode of a SPCE to exhibit an enough hydrophilic surface for appropriate interaction with the biological target as well as the following enzyme-assisted amplification. Water contact angle measurement was used to observe the wettability of an electrode surface determined by the shape of a water droplet, which designates a surface hydrophobic when the contact angle is greater than 90^0 (Law 2014). **Figure 2A** showed a distinct water droplet on a bare SPCE surface with a contact angle of

118.79^0, suggesting an extremely hydrophobic surface that may hinder the aqueous biosensing process. Also, the carbon-based SPCE lacked chemical functionalization ability for the immobilization of target probes to generate a target-specific biosensing platform. We also compared with a direct gold electrodeposition on a SPCE (Au@SPCE), which was confirmed to possess not only the functionalization ability via gold-sulfur bonding, but also improved electrochemical conductivity (Jou et al. 2017). However, we found that Au@SPCE surface presented a slightly more hydrophobic surface with a contact angle of 126.31^0. The contact angle was significantly reduced to 30.12^0 on a PDA film-deposited SPCE (PDA@SPCE), which may attribute to the polar functional groups (-NH and -OH) of the PDA film that introduced hydrophilicity to the electrode surface (Lee et al. 2007; Ryu et al. 2018; Wei et al. 2017). Meanwhile, a comparable contact angle was also observed for PDA-AuNPs composite at 38.88^0. Electrochemical conductivity was studied on cyclic voltammetric behaviors of the two commonly-used electroactive molecules, $Fe(CN)_6^{3-/4-}$ and $Ru(NH_3)_6^{2+/3+}$, on a bare SPCE, and electrodes with different modifications. **Figure 2B** displayed a well-defined pair of redox peaks at 0.07 V and 0.24 V that corresponded to $Fe(CN)_6^{3-/4-}$ on a bare SPCE; however, such peaks for other modified electrodes were no longer distinct, along with substantial electrochemical current decline. Besides, the poor electrochemical reversibility of the modified electrodes were observed, as evidence by that the redox potential difference of $Fe(CN)_6^{3-/4-}$ molecules ascended from 0.17 V to 0.8 V as for a bare SPCE and the modified electrodes, respectively. The phenomenon may be ascribed to the negatively-charged PDA film that electrically repelled $Fe(CN)_6^{3-/4-}$ molecules via electrostatic repulsion (Zangmeister et al. 2013). Cyclic voltammetric behavior of positively-charged $Ru(NH_3)_6^{2+/3+}$ molecules, on the other hand, showed a distinct pair of peaks for each fabricated electrode in **Figure 2C**. More importantly, higher reduction/oxidation current that was acquired by the PDA-AuNPs@SPCE improved conductivity as compared with the bare SPCE and the PDA@SPCE. The resulting PDA-AuNPs@SPCE was therefore

able to be sensitized with amine-functionalized electrode probes via cross-linkage with glutaraldehyde (GA). Characterization made by gel electrophoresis provided additional evidence on the negative charge of PDA. Also, the grafting of the electrode probe (EP) on PDA-AuNPs composite (EP/PDA-AuNPs) was characterized using gel electrophoresis. **Figure 2D** showed that the band positions of EP/PDA-AuNPs (lane 3) and EP/PDA (lane 5) composites were both higher than that of EP only (lane 1), confirming a successful grafting of EP via GA-mediated cross-linkage. In addition, the visual detection of higher band position of EP/PDA composite also validated the negative charge of the PDA film as that of the DNA backbone of EP, making the whole EP/PDA composite could be easily pull-down to the anode based on electrostatic attraction. Collectively, the charge property of the PDA-AuNPs composite characterized by the gel electrophoresis provided an additional verification on the negative charge carried by the PDA-Au composite, in consistency with that by the aforementioned cyclic voltammetry measurements.

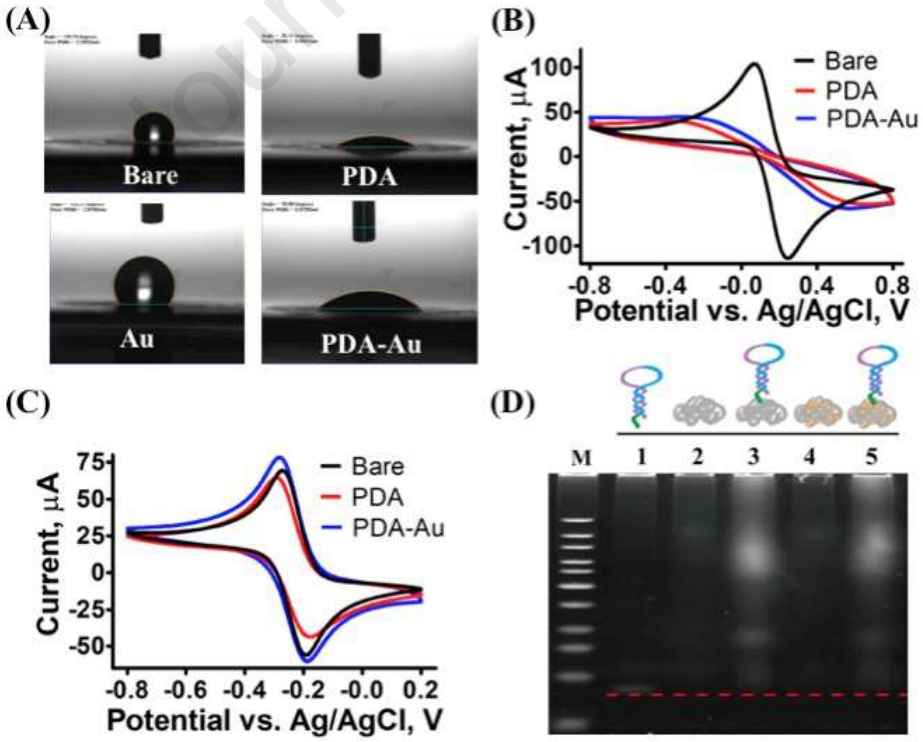

Figure 2. Characterization of a bare SPCE and different modified-SPCEs by **(A)** water contact angle measurements and cyclic voltammetric measurements using **(B)** $Fe(CN)_6^{3-/4-}$ and **(C)** $Ru(NH_3)_6^{2+/3+}$

electroactive redox probes. **(D)** Gel electrophoresis analysis (15%) of the conjugation of electrode probe (EP) via glutaraldehyde linkage. M indicates the DNA markers for 10 – 300 bp. Lane 1: 100 nM EP, Lane 2: PDA polymer, Lane 3: EP-PDA conjugate, Lane 4: PDA-Au composite, Lane 5: EP-PDA-Au conjugate.

3.3 Dual-amplification strategy on the biosensing of target miR-196b

A hairpin-structured probe was designed to specifically detect the pancreatic cancer-associated target miR-196b (22 nucleotides), of which the complementary sequence was included in the target probe hairpin (TP) with six nucleotides in the loop region and the 16 nucleotides in the stem region (**Scheme 1B**). The most sequences that were complementary to the target, was caged in the stem region to ensure the stability of the TP conformation, while the six nucleotides served as a toehold to kinetically increase its hybridization ability with the target miR-196b (Srinivas et al. 2013). Upon reaction with target miR-196, the TP opened on hybridization as a result of a higher band due to the T/TP duplex formation, shown in the lane 5 of **Figure 3**. Simultaneously, the released strand in the stem of the TP therefore triggered another opening of a hairpin-structured electrode probe by sequence complementarity. It was worth noting that the stability of the EP was crucial; that is, the hybridization of EP/TP duplex should be prohibited in the absence of target miR-196 (T). The lane 6 of **Figure 3** validated that both the TP and EP maintained great stability as in the hairpin structures, and no additional band formations that may suggest the non-specific hybridization between a target probe (TP) and an electrode probe (EP). Once target miR-196b was present, however, the biosensing event occurred at the formation of T/TP duplex, and a dual signal amplification reaction was initiated subsequently. The opening of hairpin-structured EP by the T/TP duplex launched a polymerase-assisted signal amplification by having the hybridized EP as a primer to elongate on the TP that served as a template, followed by the polymerization of a serial guanine-rich (G-rich) sequence. The generated G-rich sequence, after de-hybridization from the EP by the treatment of urea and the intercalation of hemin, was able to perform peroxidase-like activity

catalyzing TMB/H_2O_2 reaction. The implement of Klenow fragment polymerase (3'-> 5' exo) served two purposes in the dual signal amplification. For one was the EP-primed polymerization into signal-producing G-rich sequences, and the other was the strand displacement that displaced the pre-hybridized target on the TP, liberating the target to find another TP so as to initiate a next polymerization and strand displacement reaction. The two purposes of KF were validated as compared for the absence and presence of KF as in the lane 7 and 9 of **Figure 3A,** respectively. The implement of KF proved that the polymerization resulted in the generation of an elongated EP, confirmed by a denaturing gel in **Figure 3B**. In addition, the target-recycling amplification was versified by an increased consumption of EP through the KF-assisted target displacement. The sensitization of EP on a PDA-AuNPs@SPCE, aside from exerting a primer for G-rich sequence-containing elongation, enabled the translation of the target-recognition event into a quantitative electrical signal.

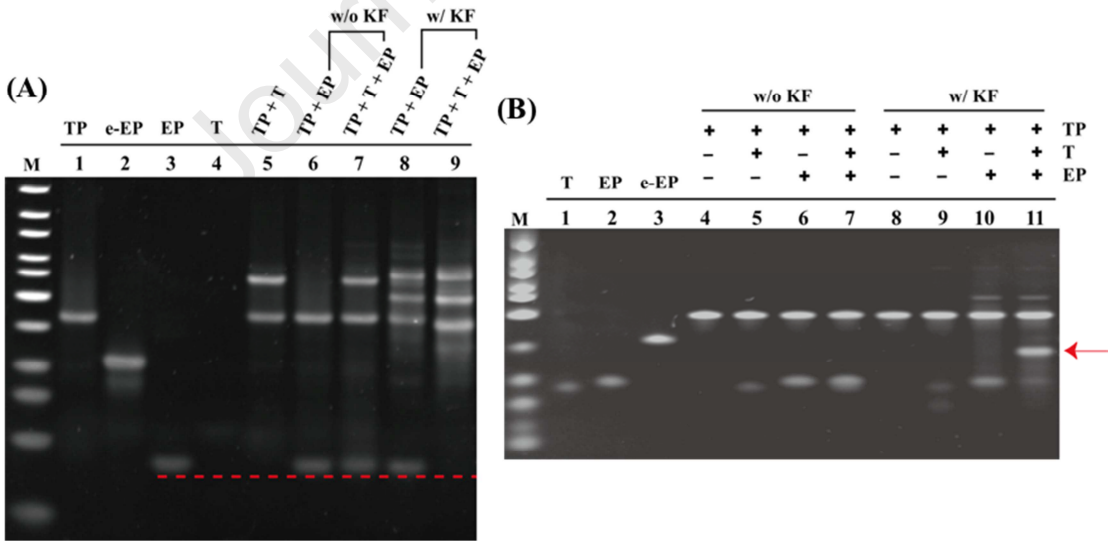

Figure 3. Gel electrophoresis analyses of the translational biosensing event between a target miR-196b and a target probe via KF-assisted dual amplification for the detection of target miR-196b using a **(A)** native gel and **(B)** 7 M urea denaturing gel (run at 55 ^{o}C, 80 V, 100 min). M indicates the DNA markers for 10 – 300 bp. Each lane: 100 nM.

3.4 Translation of biosensing process into electrochemical interface

To enable the electrochemical biosensing translation, the resulting G-rich-containing elongated EP needed to set free from the hybridized-TP-template so as to self-fold into an active hemin/G-quadruplex DNAzyme for catalyzing the electrochemical reaction of TMB molecules. Since a safer de-hybridization on a nucleic acid duplex could be achieved by the use of urea, different concentration of urea was initially analyzed in free solution (Kourilsky P Fau - Manteuil et al.). Instead of recording the oxidized, blue TMB product upon DNAzyme catalyzing reaction, a stable form of a yellow product at wavelength of 450 nm was commonly monitored to investigate the urea-based de-hybridization approach. We firstly evaluated the effect of different concentrations of urea (0, 0.05, 1, 2.5, 4 M) on the absorption measurement for the yellow TMB product, and confirmed that the presence of urea was not a point at issue (**Figure S1**). We perceived that 4 M of urea was left deposited on a working electrode after a standard between-step wash-and-dry procedure, and the residue of urea could severely interfere with the electrochemical signal acquisition. A low concentration range of urea (0.05, 1, 2.5 M) was therefore preferably selected to further examine the de-hybridizing capability for a synthetic e-EP/TP duplex, where an elongated EP (e-EP) consisting of G-rich sequence was hybridized with a target probe (TP) beforehand. Determination of the absorbance change of the TMB/H_2O_2 catalytic reaction was consequently employed to identify an optimal urea concentration for the de-hybridization of a synthetic e-EP/TP duplex. **Figure 4A** showed that 0.05 M and 1 M of urea was able to de-hybridize the synthetic TP/e-EP duplex, so that the released e-EP was able to self-fold into active DNAzyme in catalyzing TMB as expected, judging by the comparable absorbance values acquired with that of the synthetic single-stranded e-EP (black bar, a positive control group). Besides, 1 M of urea was found to be the optimum concentration to fully depart the e-EP from the T/e-EP duplex so as to restore its catalytic ability based on the highest signal-to-noise ratio (approximately 2.78). A negative control group

(green bar), represented by the absorbance resulting from the TP/e-EP duplex in the absence urea, validated that the duplex formation indeed prohibited the e-EP from catalyzing the oxidation of TMB in **Figure 4B**. Upon the treatment of urea, on the contrary, the TP/e-EP duplex (blue bar) exhibited a distinct absorbance change by ~ 0.14 a.u., and the optical change was equivalent to that achieved by using a synthetic, single-stranded e-EP (yellow bar). Therefore, the treatment of urea was able to not only release the e-EP from the TP/e-EP duplex, but also to restore the e-EP to its full catalytic ability. After confirmation in a free solution fashion, an EP/PDA-AuNPs@SPCE was subjected to a pre-reacted T/TP duplex solution to establish a T/TP/EP/PDA-AuNPs@SPCE format, followed by the treatment of urea and characterized by cyclic voltammetric (CV) measurements in **Figure 4C**. A well-superposed CV curves obtained from the urea-treated SPCE and the EP/PDA-AuNPs@SPCE implied the treatment of urea was also applicable on the electrode. To maximize the efficiency in the target-recycling-amplification strategy as a result of an amplified generation of elongated EP, the amount of KF and the reaction time were varied and accordingly evaluated to obtain the optimal conditions of 0.5 U/μL and 120 min, respectively (data not shown).

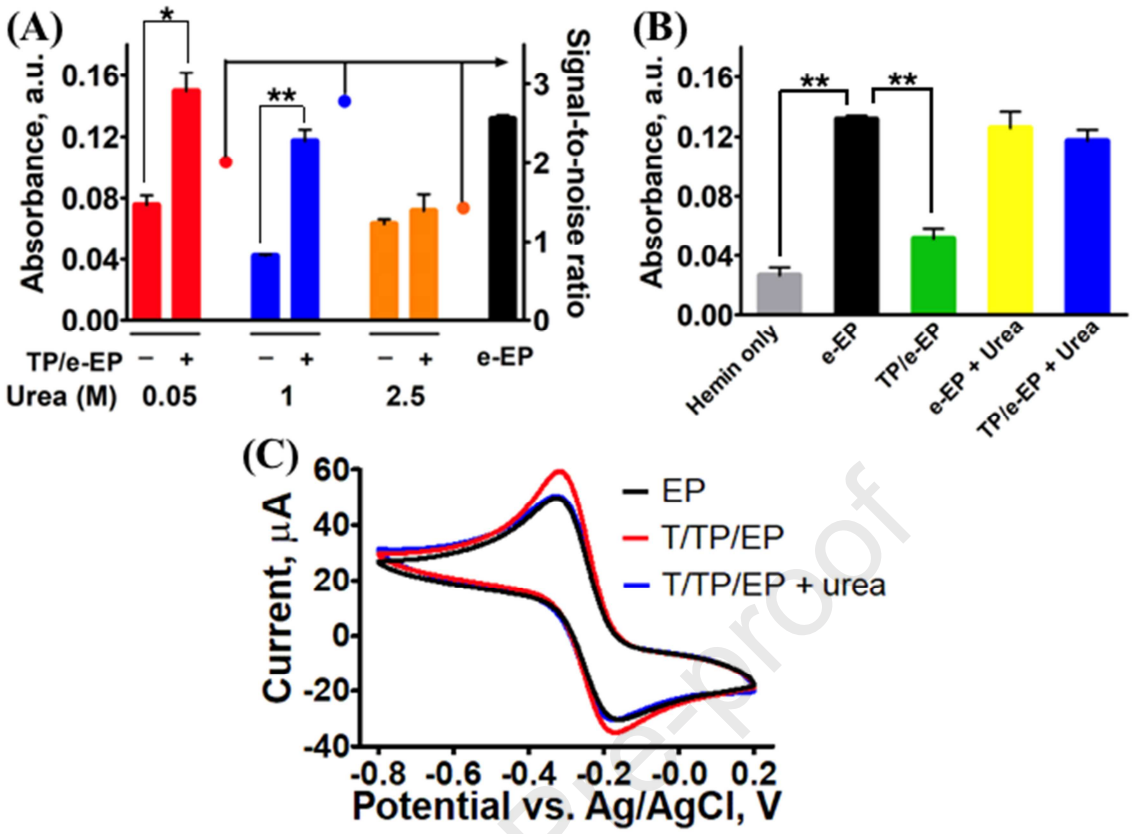

Figure 4. Assessment of de-hybridization ability of urea. **(A)** Different concentrations of urea (0.05, 1, 2.5 M) were used to treat a synthetic TP/e-EP duplex solution, and the resulting solution was assessed for the catalytic ability of e-EP in catalyzing TMB/H_2O_2 system by UV-VIS spectral measurements. The signal-to-noise ratio (right y-axis) was obtained by dividing the presence of TP/e-EP to the absence of TP/e-EP. **(B)** Comparison of the catalytic ability of hemin only, single-stranded e-EP in the absence (black bar) and presence (yellow) of urea, and TP/e-EP duplex in the absence (green bar) and presence of urea (blue bar). **(C)** Cyclic voltammetric measurements of $Ru(NH_3)_6^{3+}$ redox molecules to compare the different reaction formats on the basis of a PDA-Au@SPCE. Error bars derived from N = 3 measurements. *indicated statistical significance with p-value less than 0.05 under 95% confidence level, and **indicated the p-value less than 0.01 under 95% confidence level

3.5 Performance of an integrated electrochemical biosensor and its application in real sample

The successful integrated electrochemical biosensor enabled the biosensing of the target miR-196b as well as the translation into an electrochemical signal output. The obtained cathodic currents at 0.26 V and 0.4 V were attributed to the electro-reduction of TMB by the generated hemin/G-quadruplex DNAzyme, where TMB involved a two-electron electro-reduction process (Campuzano et al. 2019). Various concentrations of synthetic target miR-196b were examined in

Figure 5A, displaying a concentration-dependent signal increase. The corresponding signal change (ΔCurrent) at 0.26 V was used to establish a calibration curve by plotting the current difference against the logarithm of the concentration of miR-196b from 1.0 pM to 10 nM. The linear relationship was described by the equation showing ΔCurrent (μA) = $\mathbf{1.22 \log C_{miR-196b} - 0.317}$ ($\boldsymbol{R^2 = 0.98}$), and the limit of detection was calculated to be 0.26 pM, calculated by three times standard deviation from average of the blank (without miR-196b) (Purohit et al. 2020). In addition, coefficient of variance (CV) was calculated to be 8.5 ± 3.1%, showing that the proposed biosensor exhibited a nice analytical reproducibility toward the detection of miR-196b. To examine whether the proposed biosensor was able to discriminate target miR-196b, selectivity performance of the proposed biosensor was also investigated for different synthetic miRNA analogs that were DNA backbones with the same sequence, except thymine substituted for uracil. The sequence complementarity between DNA-DNA homoduplex was stronger than DNA-RNA heteroduplex, which may increase the selectivity challenge. In particular, a comparison on DNA-21 was of great importance because it was commonly found in all cancer-associated biological environments. The proposed biosensor showed a good selectivity in discriminating different miRNA analogs in **Figure 5B.** The biosensor was further challenged with un-diluted real human serum samples with a known spike of 0.7 attomol of synthetic miR196b. The serum spiked with 0.7 attomol miR-196b was extracted using a commercially-available kit, and detected using the proposed biosensor (**Figure S3**). The concentration was determined using the calibration curve, and a recovery rate was calculated to be 105 ± 4.1% by comparison to the same known amount-spiked buffer sample. The satisfactory recovery rate strongly confirmed the proposed biosensor for efficient detection of target miR-196b in real biological sample, and the performance was compared with recent electrochemical biosensors for miRNA detection in **Table S1.** As a result, the dual amplification strategy for

translational electrochemical detection of pancreatic cancer-related miR-196b implied tremendous potential for serving an alternative diagnostics for miRNA-related cancers.

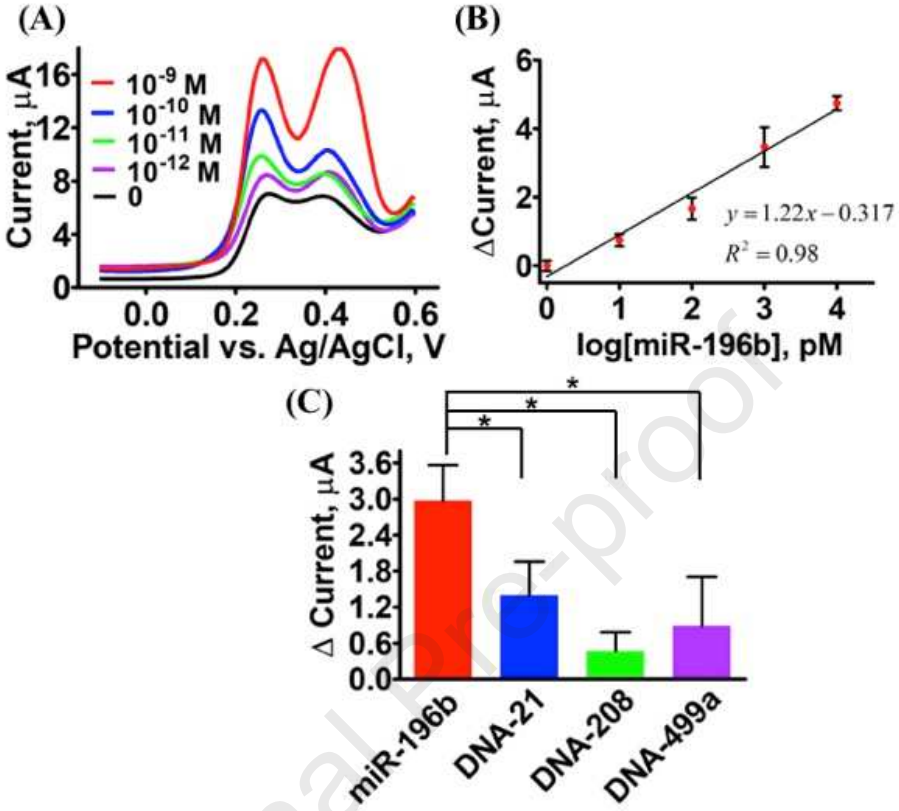

Figure 5. (A) SWV curves corresponding to the analysis of various concentrations of target miR-196b and **(B)** the derived calibration curve based on the current difference (ΔCurrent) and various concentrations of target. The current difference (ΔCurrent) at a potential of 0.26 V was subtracted from the current of the absence of target miR-196b. Error bars derived from N = 3 measurements. **(C)** Detection of other common miRNA DNA-backbone analogues using the proposed biosensor. Error bars derived from N = 3 measurements. *indicated statistical significance with p-value less than 0.05 under 95% confidence level

4. Conclusions

In conclusion, we have successfully fabricated an electrochemical biosensing platform for sensitive detection of pancreatic-cancer associated miR-196b based on a PDA-AuNPs composite, where an in-situ reduction of gold nanoparticles during the process of polydopamine self-polymerization in alkaline buffered solution. In addition, the resulting hydrophilic PDA-AuNPs-modified screen-printed electrode served as an easy-to-functionalize interface to immobilize an electrode probe for translating a target-triggered biosensing event into an electrochemical signal.

The proposed biosensor exhibited good sensitivity and selectivity toward miR-196b with detection limit of 0.26 pM, which attributed to the single polymerase-boosted dual amplification reaction by the generation of a guanine-rich (G-rich) single-stranded DNA product. The generation of G-rich product created a primary amplification as a result of target recycling, and a secondary amplification due to non-enzymatic catalysis of TMB/H_2O_2. The proposed biosensor also demonstrated the capability of real sample analysis, with a recovery rate of 105 ± 4.1% performed in a spiked human serum sample. Although a future challenge may lie in the comparison to the reference gene analysis technologies (Geiss et al. 2006), great promise as a screening tool as a point-of-care testing for aggressive cancer.

Supplementary Information

The supplementary Information is available free of charge on the Elsevier website at https://doi.org/xxxxxx for the employed sequence of oligonucleotides, the image of a screen-printed electrode, and the effect of urea on the absorption measurement, the electrochemical detection of target miR-196b in a spiked-serum sample in comparison to that in a buffer sample, and a table for the performance comparison with recent electrochemical biosensors for the detection of miRNA (PDF).

Author information

Corresponding Author

Dr. Amily Fang-Ju Jou – *Department of Chemistry, Chung Yuan Christian University, No. 200, Chung Pei Road, Chung Li District, Taoyuan City 320314, Taiwan (ROC);* Phone: +886-3-2653346

Email: afjjou@cycu.edu.tw

Authors

Mr. SSu-Chia Chen – *Department of Chemistry, Chung Yuan Christian University, No. 200, Chung Pei Road, Chung Li District, Taoyuan City 320314, Taiwan (ROC)*

Ms. Kuan-Ting Chen – *Department of Chemistry, Chung Yuan Christian University, No. 200, Chung Pei Road, Chung Li District, Taoyuan City 320314, Taiwan (ROC)*

Author Contributions

† SSu-Chia Chen and Kuan-Ting Chen contributed equally to this work.

Acknowledgements

This work was supported by the Taiwan Ministry of Science and Technology [grant number: MOST 107-2113-M-033-010-MY2 and 109-2113-M-033-003-]. The authors thanked Prof. Jhy-Der Chen for the use of FT-IR spectroscopy, and Prof. Jui-Ming Yeh for the use of water contact angle measurement setup.

Conflict of Interest Disclosure

The authors declare no conflict of interest relevant to this article.

References

Ali, M.M., Li, F., Zhang, Z., Zhang, K., Kang, D.-K., Ankrum, J.A., Le, X.C., Zhao, W., 2014. Rolling circle amplification: a versatile tool for chemical biology, materials science and medicine. Chemical Society Reviews 43(10), 3324-3341.

Bryant, R.J., Pawlowski, T., Catto, J.W.F., Marsden, G., Vessella, R.L., Rhees, B., Kuslich, C., Visakorpi, T., Hamdy, F.C., 2012. Changes in circulating microRNA levels associated with prostate cancer. British Journal of Cancer 106(4), 768-774.

Campuzano, S., Pedrero, M., González-Cortés, A., Yáñez-Sedeño, P., Pingarrón, J.M., 2019. Electrochemical biosensors for autoantibodies in autoimmune and cancer diseases. Analytical Methods 11(7), 871-887.

Chandra, P., Tan, Y.N., Singh, S.P., 2017. Next Generation Point-of-care Biomedical Sensors Technologies for Cancer Diagnosis, 1 ed. Springer Singapore.

Choi, H.M.T., Beck, V.A., Pierce, N.A., 2014. Next-Generation in Situ Hybridization Chain Reaction: Higher Gain, Lower Cost, Greater Durability. ACS Nano 8(5), 4284-4294.

Christodouleas, D.C., Kaur, B., Chorti, P., 2018. From Point-of-Care Testing to eHealth Diagnostic Devices (eDiagnostics). ACS Central Science 4(12), 1600-1616.

Dai, J., He, H., Duan, Z., Guo, Y., Xiao, D., 2017. Self-Replicating Catalyzed Hairpin Assembly for Rapid Signal Amplification. Analytical Chemistry 89(22), 11971-11975.

Evans, J., Chapple, A., Salisbury, H., Corrie, P., Ziebland, S., 2014. "It can't be very important because it comes and goes"--patients' accounts of intermittent symptoms preceding a pancreatic cancer diagnosis: a qualitative study. BMJ Open 4(2), e004215-e004215.

Ge, Z., Lin, M., Wang, P., Pei, H., Yan, J., Shi, J., Huang, Q., He, D., Fan, C., Zuo, X., 2014. Hybridization Chain Reaction Amplification of MicroRNA Detection with a Tetrahedral DNA Nanostructure-Based Electrochemical Biosensor. Analytical Chemistry 86(4), 2124-2130.

Geiss, G.K., Bumgarner Re Fau - Birditt, B., Birditt B Fau - Dahl, T., Dahl T Fau - Dowidar, N., Dowidar N Fau - Dunaway, D.L., Dunaway Dl Fau - Fell, H.P., Fell Hp Fau - Ferree, S., Ferree S Fau - George, R.D., George Rd Fau - Grogan, T., Grogan T Fau - James, J.J., James Jj Fau - Maysuria, M., Maysuria M Fau - Mitton, J.D., Mitton Jd Fau - Oliveri, P., Oliveri P Fau - Osborn, J.L., Osborn Jl Fau - Peng, T., Peng T Fau - Ratcliffe, A.L., Ratcliffe Al Fau - Webster, P.J., Webster Pj Fau - Davidson, E.H., Davidson Eh Fau - Hood, L., Hood L Fau - Dimitrov, K., Dimitrov, K., 2006. Direct multiplexed measurement of gene expression with color-coded probe pairs. Nature Biotechnology 26(3), 317-325.

Gilles, M.-E., Hao, L., Huang, L., Rupaimoole, R., Lopez-Casas, P.P., Pulver, E., Jeong, J.C., Muthuswamy, S.K., Hidalgo, M., Bhatia, S.N., Slack, F.J., 2018. Personalized RNA Medicine for Pancreatic Cancer. Clinical Cancer Research 24(7), 1734.

Heneghan, H.M., Miller, N., Lowery, A.J., Sweeney, K.J., Newell, J., Kerin, M.J., 2010. Circulating microRNAs as novel minimally invasive biomarkers for breast cancer. Annals of Surgery 251.

Janovák, L., Dékány, I., 2010. Optical properties and electric conductivity of gold nanoparticle-containing, hydrogel-based thin layer composite films obtained by photopolymerization. Applied Surface Science 256(9), 2809-2817.

Jou, A.F.-J., Chen, Y.-J., Li, Y., Chang, Y.-F., Lee, J.-j., Liao, A.T., Ho, J.-a.A., 2017. Target-Triggered, Dual Amplification Strategy for Sensitive Electrochemical Detection of a Lymphoma-associated MicroRNA. Electrochimica Acta 236(10), 190-197.

Kanno, S., Nosho, K., Ishigami, K., Yamamoto, I., Koide, H., Kurihara, H., Mitsuhashi, K., Shitani, M., Motoya, M., Sasaki, S., Tanuma, T., Maguchi, H., Hasegawa, T., Kimura, Y., Takemasa, I., Shinomura, Y., Nakase, H., 2017. MicroRNA-196b is an independent prognostic biomarker in patients with pancreatic cancer. Carcinogenesis 38(4), 425-431.

Kawaguchi, T., Komatsu, S., Ichikawa, D., Morimura, R., Tsujiura, M., Konishi, H., Takeshita, H., Nagata, H., Arita, T., Hirajima, S., Shiozaki, A., Ikoma, H., Okamoto, K., Ochiai, T., Taniguchi, H., Otsuji, E., 2013. Clinical impact of circulating miR-221 in plasma of patients with pancreatic cancer. British Journal of Cancer 108(2), 361-369.

Kourilsky P Fau - Manteuil, S., Manteuil S Fau - Zamansky, M.H., Zamansky Mh Fau - Gros, F., Gros, F., DNA-RNA hybridization at low temperature in the presence of urea. Biochemical and Biophysical Research Communications 41(4), 1080-1087.

Lan, T., Zhang, J., Lu, Y., 2016. Transforming the blood glucose meter into a general healthcare meter for in vitro diagnostics in mobile health. Biotechnology Advances 34(3), 331-341.

Law, K.-Y., 2014. Definitions for Hydrophilicity, Hydrophobicity, and Superhydrophobicity: Getting the Basics Right. The Journal of Physical Chemistry Letters 5(4), 686-688.

Lee, H., Dellatore Sm Fau - Miller, W.M., Miller Wm Fau - Messersmith, P.B., Messersmith, P.B., 2007. Mussel-inspired surface chemistry for multifunctional coatings. Science 318(5849), 426-430.
Liu, Y., Li, S., Zhang, L., Zhao, Q., Li, N., Wu, Y., 2020. A sensitive and specific method for microRNA detection and in situ imaging based on a CRISPR–Cas9 modified catalytic hairpin assembly. RSC Advances 10(47), 28037-28040.
Luo, H., Gu, C., Zheng, W., Dai, F., Wang, X., Zheng, Z., 2015. Facile synthesis of novel size-controlled antibacterial hybrid spheres using silver nanoparticles loaded with poly-dopamine spheres. RSC Advances 5, 13470-13477.
Luo, J., Zhang, N., Liu, R., Liu, X., 2014. In situ green synthesis of Au nanoparticles onto polydopamine-functionalized graphene for catalytic reduction of nitrophenol. RSC Advances 4(110), 64816-64824.
Mitchell, P.S., Parkin, R.K., Kroh, E.M., Fritz, B.R., Wyman, S.K., Pogosova-Agadjanyan, E.L., Peterson, A., Noteboom, J., O'Briant, K.C., Allen, A., Lin, D.W., Urban, N., Drescher, C.W., Knudsen, B.S., Stirewalt, D.L., Gentleman, R., Vessella, R.L., Nelson, P.S., Martin, D.B., Tewari, M., 2008. Circulating microRNAs as stable blood-based markers for cancer detection. Proceedings of the National Academy of Sciences 105(30), 10513-10518.
Pallela, R., Chandra, P., Noh, H.-B., Shim, Y.-B., 2016. An amperometric nanobiosensor using a biocompatible conjugate for early detection of metastatic cancer cells in biological fluid. Biosensors and Bioelectronics 85, 883-890.
Purohit, B., Vernekar, P.R., Shetti, N.P., Chandra, P., 2020. Biosensor nanoengineering: Design, operation, and implementation for biomolecular analysis. Sensors International 1, 100040.
Qualliotine, J.R., Bolat, G., Beltrán-Gastélum, M., de Ávila, B.E.-F., Wang, J., Califano, J.A., 2019. Acoustic Nanomotors for Detection of Human Papillomavirus–Associated Head and Neck Cancer. Otolaryngology–Head and Neck Surgery 161(5), 814-822.
Rawla, P., Sunkara, T., Gaduputi, V., 2019. Epidemiology of Pancreatic Cancer: Global Trends, Etiology and Risk Factors. World Journal of Oncology 10(1), 10-27.
Ryu, J.H., Messersmith, P.A.-O.X., Lee, H.A.-O., 2018. Polydopamine Surface Chemistry: A Decade of Discovery. ACS Applied Materials & Interfaces. 10(9), 7523-7540.
Soper, S.A., Brown, K., Ellington, A., Frazier, B., Garcia-Manero, G., Gau, V., Gutman, S.I., Hayes, D.F., Korte, B., Landers, J.L., Larson, D., Ligler, F., Majumdar, A., Mascini, M., Nolte, D., Rosenzweig, Z., Wang, J., Wilson, D., 2006. Point-of-care biosensor systems for cancer diagnostics/prognostics. Biosensors and Bioelectronics 21(10), 1932-1942.
Srinivas, N., Ouldridge, T.E., Sulc, P., Schaeffer, J.M., Yurke, B., Louis, A.A., Doye, J.P.K., Winfree, E., 2013. On the biophysics and kinetics of toehold-mediated DNA strand displacement. Nucleic acids research 41(22), 10641-10658.
Wang, G., Tian, W., Liu, X., Ren, W., Liu, C., 2020. New CRISPR-Derived microRNA Sensing Mechanism Based on Cas12a Self-Powered and Rolling Circle Transcription-Unleashed Real-Time crRNA Recruiting. Analytical Chemistry 92(9), 6702-6708.
Wang, H.-L., Zhou, R., Liu, J., Chang, Y., Liu, S., Wang, X.-B., Huang, M.-F., Zhao, Q., 2017. MicroRNA-196b inhibits late apoptosis of pancreatic cancer cells by targeting CADM1. Scientific Reports 7(1), 11467.
Wei, N., Jiang, Y., Ying, Y., Guo, X., Wu, Y., Wen, Y., Yang, H., 2017. Facile construction of a polydopamine-based hydrophobic surface for protection of metals against corrosion. RSC Advances 7(19), 11528-11536.
Wen, Y., Xu, Y., Mao, X., Wei, Y., Song, H., Chen, N., Huang, Q., Fan, C., Li, D., 2012. DNAzyme-Based Rolling-Circle Amplification DNA Machine for Ultrasensitive Analysis of MicroRNA in Drosophila Larva. Analytical Chemistry 84(18), 7664-7669.

Xing, Y., Wang, P., Zang, Y., Ge, Y., Jin, Q., Zhao, J., Xu, X., Zhao, G., Mao, H., 2013. A colorimetric method for H1N1 DNA detection using rolling circle amplification. Analyst 138(12), 3457-3462.

Xu, J., Xu, N., Zhou, T., Xiao, X., Gao, B., Fu, J., Zhang, T., 2017. Polydopamine coatings embedded with silver nanoparticles on nanostructured titania for long-lasting antibacterial effect. Surface and Coatings Technology 320, 608-613.

Ye, X., Fang, X., Li, Y., Wang, L., Li, X., Kong, J., 2019. Sequence-Specific Probe-Mediated Isothermal Amplification for the Single-Copy Sensitive Detection of Nucleic Acid. Analytical Chemistry 91(10), 6738-6745.

Zangmeister, R.A., Morris, T.A., Tarlov, M.J., 2013. Characterization of Polydopamine Thin Films Deposited at Short Times by Autoxidation of Dopamine. Langmuir 29(27), 8619-8628.

Zhang, M., Peltier, R., Zhang, M., Lu, H., Bian, H., Li, Y., Xu, Z., Shen, Y., Sun, H., Wang, Z., 2017. In situ reduction of silver nanoparticles on hybrid polydopamine–copper phosphate nanoflowers with enhanced antimicrobial activity. Journal of Materials Chemistry B 5(27), 5311-5317.

Zhang, Y.-P., 2019. A modified exponential amplification reaction (EXPAR) with an improved signal-to-noise ratio for ultrasensitive detection of polynucleotide kinase. Chemical communications 55, 7611-7614.

Zheng, A.-X., Li, J., Wang, J.-R., Song, X.-R., Chen, G.-N., Yang, H.-H., 2012. Enzyme-free signal amplification in the DNAzyme sensor via target-catalyzed hairpin assembly. Chemical Communications 48(25), 3112-3114.

Zhu, Y., Chandra, P., Shim, Y.-B., 2013. Ultrasensitive and Selective Electrochemical Diagnosis of Breast Cancer Based on a Hydrazine–Au Nanoparticle–Aptamer Bioconjugate. Analytical Chemistry 85(2), 1058-1064.

Polydopamine-gold Composite-based Electrochemical Biosensor Using Dual-amplification Strategy for Detecting Pancreatic Cancer-associated MicroRNA

Highlights

- Synthesis of a functional electrode modifier of polydopamine-gold composite
- Dual-amplification strategy for detecting pancreatic cancer-related miR-196b
- Successful establishment of a translational electrochemical biosensing platform
- Subpico-molar detection limit enabled 105 ± 4.1% recovery in real human serum samples

Declaration of interests

☑ The authors declare that they have no known competing financial interests or personal relationships that could have appeared to influence the work reported in this paper.

☐The authors declare the following financial interests/personal relationships which may be considered as potential competing interests: